Available online at www.sciencedirect.com
ScienceDirect
Journal of the European Ceramic Society 31 (2011) 3087–3094
www.elsevier.com/locate/jeurceramsoc

Phase stability and electric conductivity of Er_2O_3–Nb_2O_5 co-doped Bi_2O_3 electrolyte

Tung Chou, Li-Der Liu, Wen-Cheng J. Wei *

Department of Materials Science and Engineering, National Taiwan University, Taiwan, ROC

Available online 28 May 2011

Abstract

Two oxides, Er_2O_3 and Nb_2O_3, are used to stabilize delta-phase Bi_2O_3 used as electrolyte of solid oxide fuel cell. Optimization of dopant ratio and total doping concentration (TDC) is determined by X-ray diffraction, and successfully reduce the TDC (Er + Nb) to 10–15 mol.%. Conductivities of different compositions are measured by two-probe method. The results show that highest conductivity appears at the minimum doping concentrations. Phase stability of ENSB samples with Er/Nb ratio of 2/1 and TDC of 10–20 mol.% at 650 °C up to 300 h is analyzed showing two newly formed (alpha- and gamma-) phases in the samples. Degradation of conductivity at 650 °C is studied in detail by DTA and TEM. The abnormity of lattice contraction of delta-phase is discussed.

Keywords: Ionic conductivity; Fuel cells; Defect; Electron microscopy; Bi_2O_3

1. Introduction

δ-Bi_2O_3 in fluorite structure (δ-structure) exhibits the highest oxygen-ion conductivity among the oxide conductors.[1–3] The ion conductivity of δ-Bi_2O_3 is two orders of magnitude higher than that of 8 mol.% yttrium stabilized zirconia (8YSZ) which is currently used as an electrolyte in SOFC. δ-Bi_2O_3 has high conductivity due to high oxygen vacancies in random distribution and weak Bi–O bond, which results in high oxygen mobility.[4] Therefore, using δ-Bi_2O_3 as the electrolyte of SOFC is possible at operation temperatures lower than 650 °C. However, Bi_2O_3 in δ-structure is only stable above 730 °C. When cooling below 730 °C, two metastable phases, tetragonal β-phase and bcc γ-phase, appear if appreciated amount of oxide additive is alloyed. The other stable phase, monoclinic α-Bi_2O_3, gradually appears below 730 °C. These phase transformations result in great reduction of electric conductivity.[1]

The δ-structure can be preserved to ambient temperature by doping enough amount of oxides, such as rare earth (e.g. Sm, Lu, Y),[1,4–11] and transition metal (V, Nb, Ta and W) oixdes.[1,12] Verkerk and Burggraaf[11] did a systematically investigation on the Bi_2O_3 systems with rare earth dopants (Yb–Gd). They found that by doping erbium (Er), the minimum doping concentration to stabilize δ-Bi_2O_3 is lowest among the rare earth series. $(Er_2O_3)_{0.2}$–$(Bi_2O_3)_{0.8}$ (as abbreviated as "20ESB") presents the highest conductivity among all single rare-earth dopant systems. They claimed that the mismatch of dopant cation radius to host Bi^{3+} radius induced lattice distortion. Less dopant level resulted in higher conductivity.

Double doping strategy is another idea to stabilize δ-structure. Meng et al.[13] has pointed out that the material system allows the lower doping concentration to stabilize δ-structure by doping two dopants due to thermodynamic advantage. In the case of Dy–W stabilized Bi_2O_3 (DWSB)[14,15], the doping concentration can be reduced to 12 mol.% and show a higher conductivity than that of 20ESB.

The δ-structure could be stabilized to ambient temperature, sluggish phase transformations are important[16–21] during long-term aging. A typically phase transformation of Bi_2O_3–Ln_2O_3 from fcc fluorite to rhombohedral occurs below 700 °C and most rapid at 600–650 °C. This transformation causes the degradation of conductivity and possibly induces other defects (e.g. microflaws). Moreover, Watanabe[22] claimed that δ-Bi_2O_3 could

* Corresponding author at: 1 Roosevelt Rd. Section 4, Taipei 106, Taiwan, ROC. Tel.: +886 2 33661317; fax: +886 2 23634562.
E-mail address: wjwei@ntu.edu.tw (W.-C.J. Wei).

0955-2219/$ – see front matter © 2011 Elsevier Ltd. All rights reserved.
doi:10.1016/j.jeurceramsoc.2011.04.016

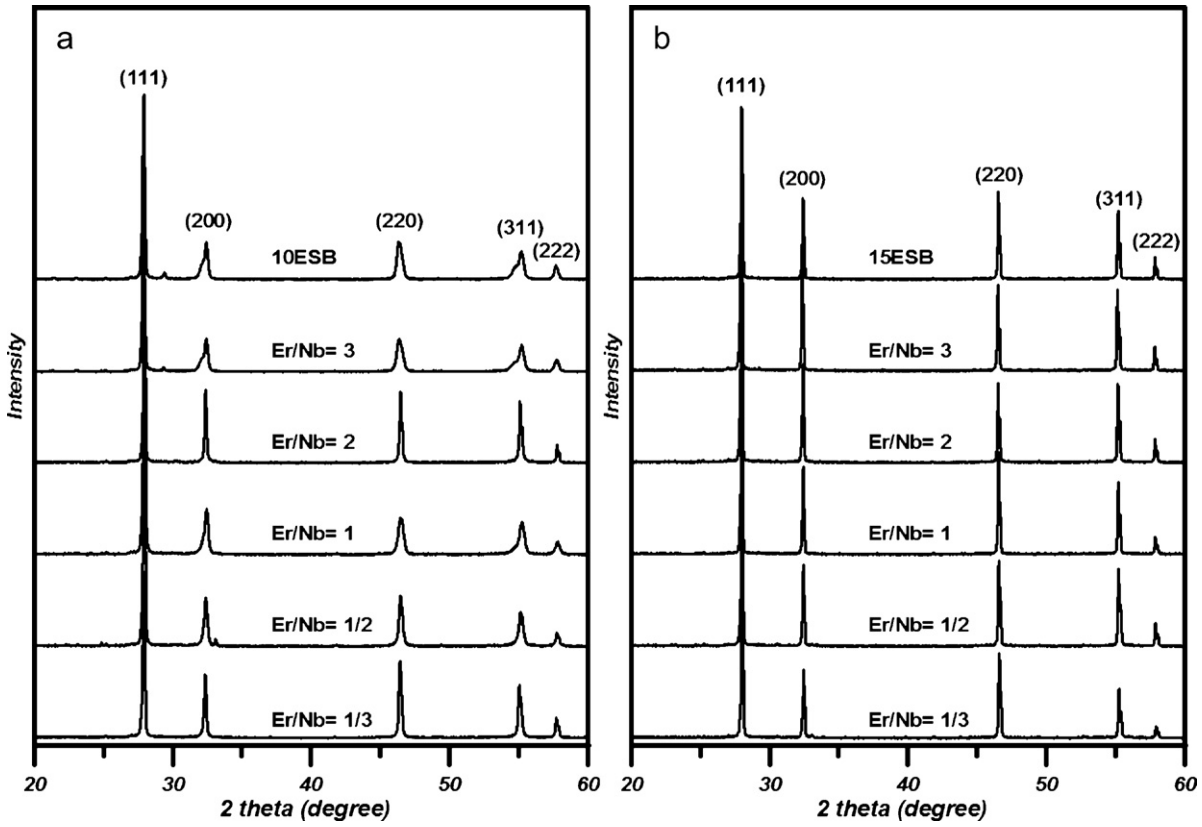

Fig. 1. XRD patterns of ENSB (a) with a fixed 10 mol.% and (b) with a fixed 15 mol.% total doping concentration (TDC). 10ESB and 15ESB mean the Bi_2O_3 samples with 10 and 15 mol.% Er_2O_3 doping level, respectively.

not be stabilized by any oxide addition in long-term aspect. The stabilized bismuth oxides were treated as a quench-in phase, in other words, meta-stabilized phase.

Jiang and Wachsman[23] did a systematically research on the effects of rare earth dopant Bi_2O_3–Ln_2O_3 (Ln = Dy, Ho, Er, Tm, and Yb) and found that the degradation rate of conductivity depended on the ion radii and doping concentration. They also observed two different mechanisms of degradation. One is phase transformation from fluorite to rhombohedral which occurs most rapidly at about 650 °C, the other one is the vacancies reversible order-disorder transformation which occurs at about 500 °C.

The other reports claimed little degradation. Fung and Virka[21] reported that the 5 mol.% ZrO_2-doped Bi_2O_3 presents only a few percents of conductivity drop during long-term annealing. Watanabe and Sekita[24] claimed that they found a composition domain of Bi_2O_3–Er_2O_3–WO_3 system, of which the composition can be truly stabilized in δ-structure. The composition $(Bi_2O_3)_{0.705}$–$(Er_2O_3)_{0.245}$–$(WO_3)_{0.050}$ performed no degradation of conductivity by annealing at 600 °C for 1000 h.

In this research, Er_2O_3 and Nb_2O_5 are used as dopants. The optimal dopant ratio and concentration are systematic investigated based on stabilization of the δ-structure. The relationship between long-term stability of the conductivity and total doping concentration of Bi_2O_3–Er_2O_3–Nb_2O_5 system (as abbreviated as "ENSB") are studied by annealing at 650 °C. Therefore, optimal dispersion of powder mixture and pressure filtration to

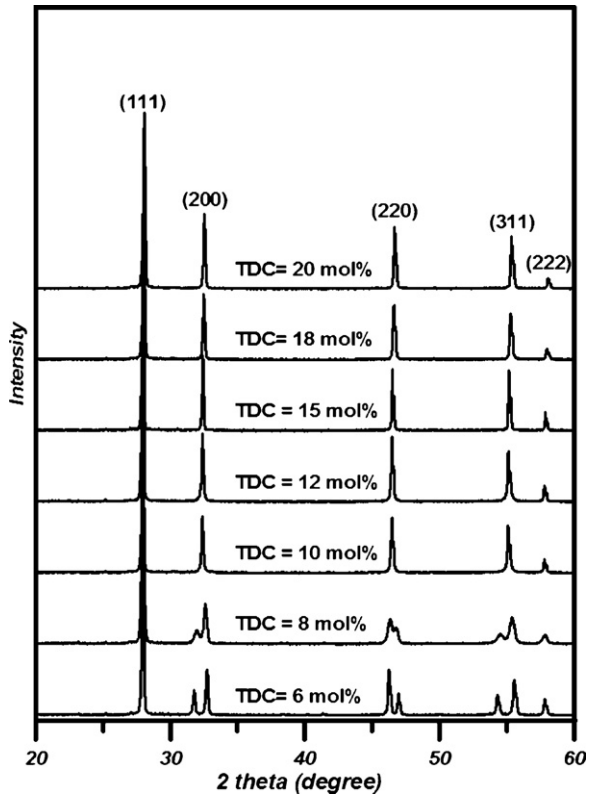

Fig. 2. XRD patterns of ENSB doped with various total doping concentrations with a fixed doping ratio of Er/Nb = 2.

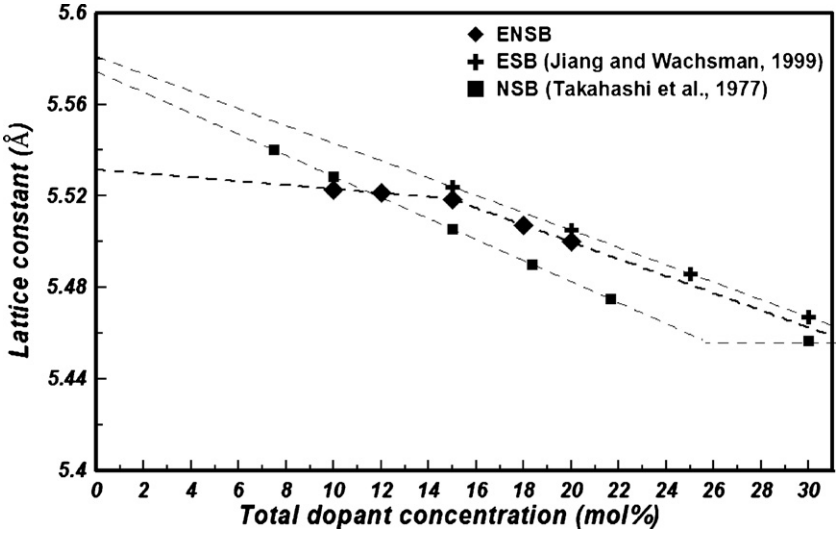

Fig. 3. Lattice constant of various ENSB compositions with a fixed doping ratio of Er/Nb = 2. The ESB[14] and NSB[12] in literature are included for comparison.

prepare uniform green samples are practiced in order to enhance the homogeneity of Bi_2O_3 electrolyte.[25]

2. Experimental

2.1. Sample preparation

Powders of Bi_2O_3 (Solartech, 99.99%), Er_2O_3 (Fu Yuan, 99.9%) and Nb_2O_5 (Alfa Aesar, 99.5%) were used to prepare slurries, then ball-milling with 5 mm zirconia grinding media in separate polyethylene bottle for 20 h. 1 wt.% (based on the powder) of dispersion agent D-134 was used for the Bi_2O_3 slurry and 2 wt.% of Darvan C was used for the Nb_2O_5. After dispersed separately, the slurries were mixed together for additional 3 h, dried and calcined at 780 °C for 10 h. The calcined powders were ground by mortar then sieved through 200-mesh screen. The sieved powders were used to prepare aqueous slurry of 28 vol.% with dispersant D-134, and mixed again with the zirconia media for 20 h. Finally, the slurries were used to prepare disk-shape pellets by pressure filtration. The pellets had a diameter of 1.0 cm and a thickness of 0.2 cm and sintered at the 870 °C for 10 h in atmosphere. All pellets had a sintered density greater than 95% theoretical density (T.D.) by Archimedes method.

The sintered pellets were polished step-by-step by SiC sand papers from #200 to #4000 mesh and cleaned in ultrasonic bath. After drying in air, only the samples for conductivity test were sputtered with Pt thin layer on both sides, then connecting Ag wires by Ag paste as electrodes.

2.2. Characterization

The crystalline structure of as-sintered and annealed samples was identified by X-ray diffraction analysis (XRD, Rigaku TTRAX III). XRD patterns were obtained at ambient temperature by using Cu Kα radiation between 20° and 60° (2θ) with scanning rate of 5°/min. The XRD patterns were indexed by the program JADE5 which included the functions of phase identification and *d*-spacing calculation. The microstructures and phase identification of annealed samples were observed by scanning electron microscopy (SEM, JEOL JSM-6510) and transition electron microscope (TEM, Philips Tecnai G^2).

Conductivities of sintered samples were measured by two-probe DC method. The temperature range was selected from 400 °C to 700 °C and tested at each 50 °C step. Every temperature step was kept at least 5 min to reach equilibrium. The resistance was read by 7555 Digital Multimeter (Yokogawa) and converted to conductivity by considering the area of electrode and thickness of electrolyte as follows:

$$\sigma = \frac{t}{RA}, \tag{1}$$

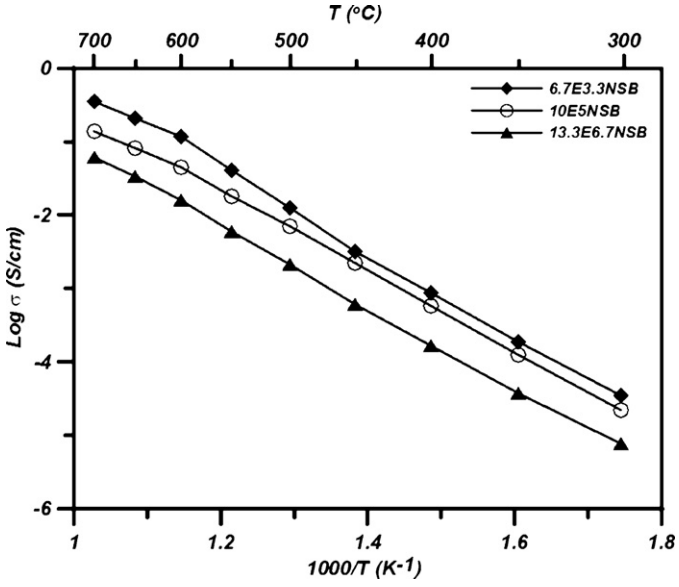

Fig. 4. Conductivities of three samples in the composition of 6.7E3.3NSB, 10E5NSB and 13.3E6.7SB plotted against 1/*T*.

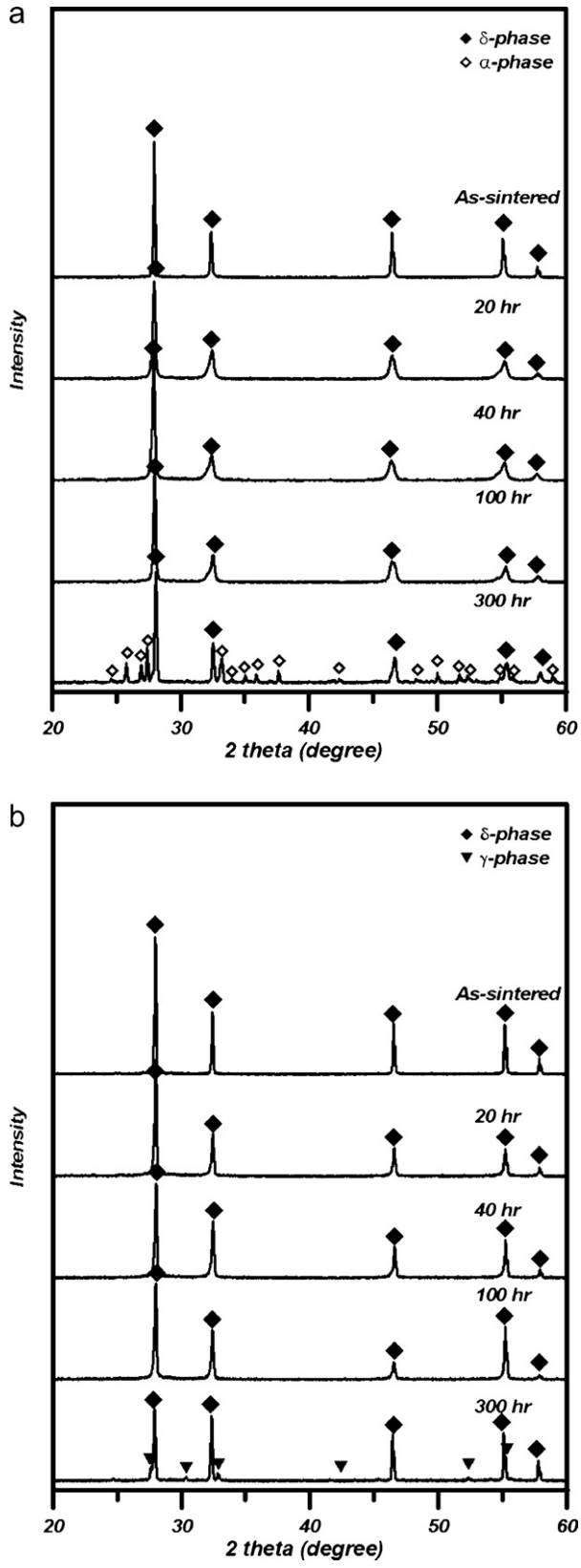

Fig. 5. XRD patterns of (a) 6.7E3.3NSB, (b) 10E5NSB and (c) 13.3E6.6NSB annealed at 650 °C for 0, 20, 40, 100 and 300 h.

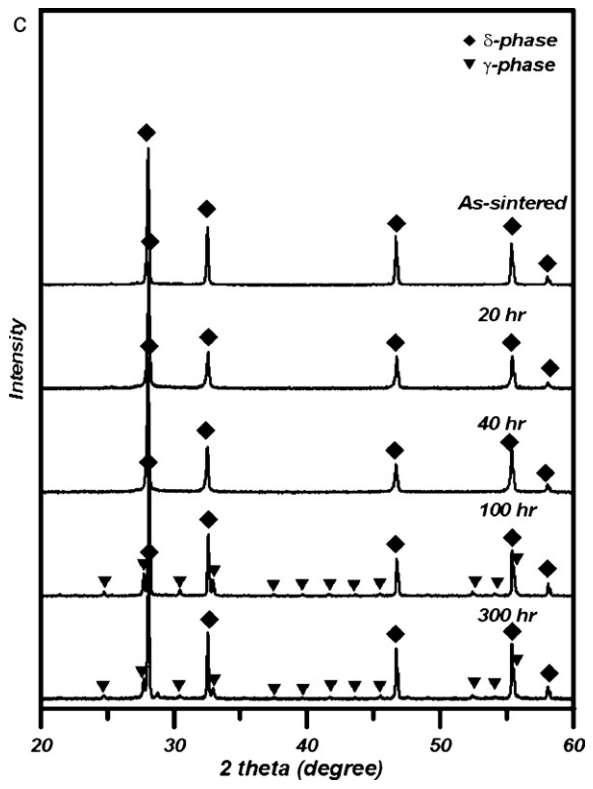

Fig. 5. (*Continued*)

where σ and R are the conductivity and resistance of electrolyte, t and A are the thickness of electrolyte and the area of electrode, respectively.

The thermal behavior of the annealed samples was investigated by differential thermal analysis (DTA, TA SDT-Q600). The samples heated in 10 °C min^{-1} in platinum crucible in air atmosphere.

3. Results and discussion

3.1. Phase stabilization

In order to find the best dopant ratio and concentration, five different Er/Nb ratios 3:1, 2:1, 1:1, 1:2 and 1:3 were tested. Fig. 1 shows the XRD patterns of the samples with fixed amount of total dopant, either 10ESB or 15ESB. The results in Fig. 1(a) shows that δ-structure can be retained to ambient temperature when the dopant ratio is Er/Nb = 2. However, for the other samples with 10 mol.% total dopant concentration (TDC), a small amount of secondary phase becomes evident. The sample of Er/Nb = 1/3 also shows good ability to stabilize the δ-phase, but the sample with Er_2O_3-rich ratio (Er/Nb = 2) are rich in oxygen vacancy, possibly perform higher ionic conductivity. Fig. 1(b) shows the XRD patterns with TDC fixed at 15 mol.% and all ratios can stabilize δ-phase, including 15ESB.

Based on the results from Fig. 1, the samples with TDC from 6 to 20 mol.% with same dopant ratio Er/Nb = 2 are tested and shown in Fig. 2. The minimum TDC of ENSB is reduced to

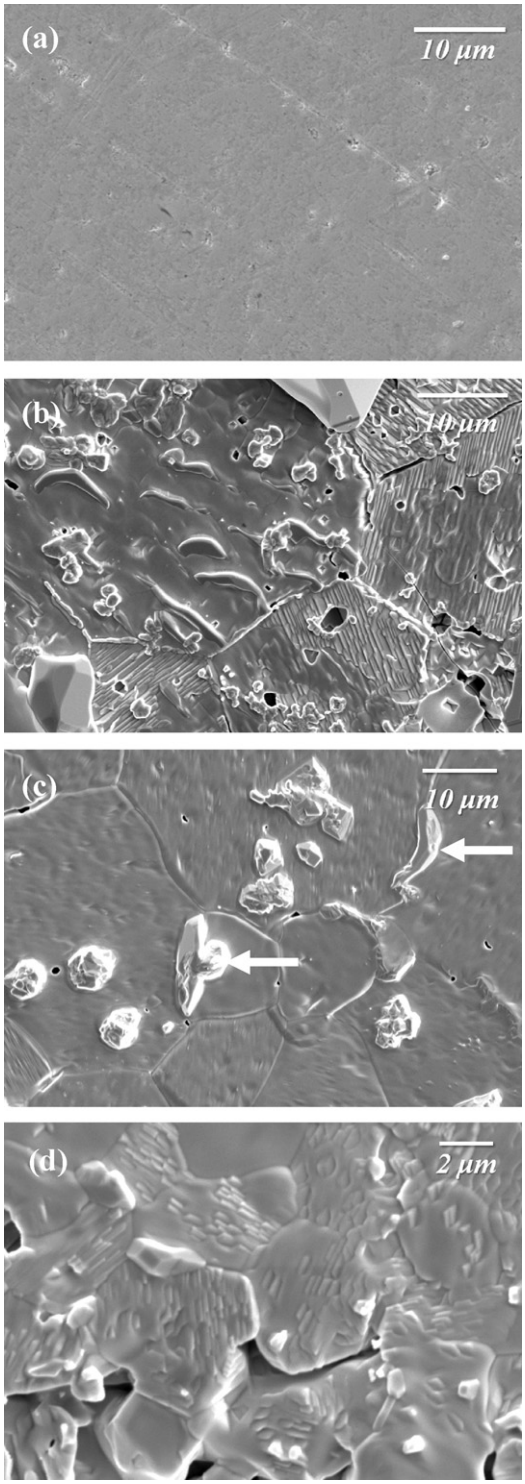

Fig. 6. SEM micrographs illustrating the surface morphologies of the samples (a) as-sintered 13.3E6.7NSB, (b) 6.7E3.3NSB, (c) 10E5NSB and (d) 13.3E6.7ESB annealed at 650 °C for 300 h.

10 mol.% enough to prevent the formation of secondary phase, i.e. β-phase shown in cooling process.

The lattice constant of the fluorite ENSB of various TDC with same dopant ratio Er/Nb = 2 were determined from three strongest peak positions and shown by an average value. The diffraction signal was obtained from the interior of the samples, which were all polished to remove the skin and to avoid the possible Bi evaporation from the surface. Fig. 3 shows the lattice constant of ENSB with various TDC at ambient temperature. The ion radii of Er^{3+} (1.004 Å) and Nb^{5+} (0.74 Å) are smaller than that of Bi^{3+} (1.17 Å). The lattice constant of ENSB decreases with increasing TDC.

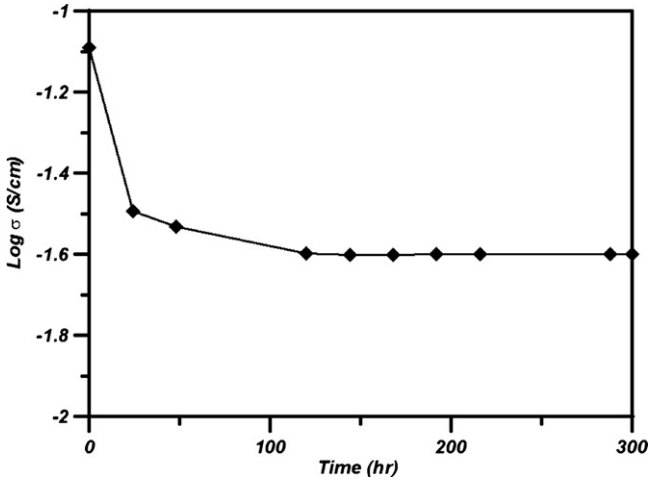

Fig. 7. Time dependant conductivity for 10E5NSB annealed at 650 °C as a function of time.

Comparing to ESB,[23] the ENSB materials showed a different lattice contraction behavior. The abnormity (discontinuity) is found at TDC of 15 mol.%. For the TDC larger than 15 mol.%, the lattice constant lies in between those of ESB and NSB, and closer to the ESB. It due to the dopant ratio Er/Nb = 2. When the TDC is less than 15 mol.%, ENSB has a smaller dependence of lattice constant on dopant concentration. It could be the co-existed behavior of two phases for the TDC = 10–15 mol.%. The lattice constant is also controlled by the presence of other phase. However, no evident of any second phase is observed in the quench-in samples, as shown in Fig. 2.

The other possibility is the amount of oxygen vacancies. When Nb_2O_5 is added into Bi_2O_3, the defect chemical reaction can be written as below:

$$Nb_2O_5 2\dot{V} = 2Nb_{Bi} + 2O_{Bi}^{x} + \frac{1}{2}O_{2(g)} \quad (2)$$

The amount of oxygen vacancies deceases with increasing the doping concentration of Nb_2O_5, but not for Er_2O_3. High content of oxygen vacancies concentration may have structural instability, and tend to form low symmetric α-structure. The lattice contraction behavior is certainly different when the vacancy content reduced to the level and favored the phase transformation of δ-to-α structure. The evidence of abnormality will be presented with the results of long-term annealing in following sections.

3.2. Electric conductivity

The conductivity results of three ENSB samples (6.7E3.3NSB, 10E5NSB, 11.25E3.75NSB) are shown in Fig. 4. The results of 6.7E3.3NSB show the best with conductivity of 0.351, 0.209, and 0.116 S cm^{-1} at 700, 600, and 500 °C, respectively. The typical trend of conductivity versus

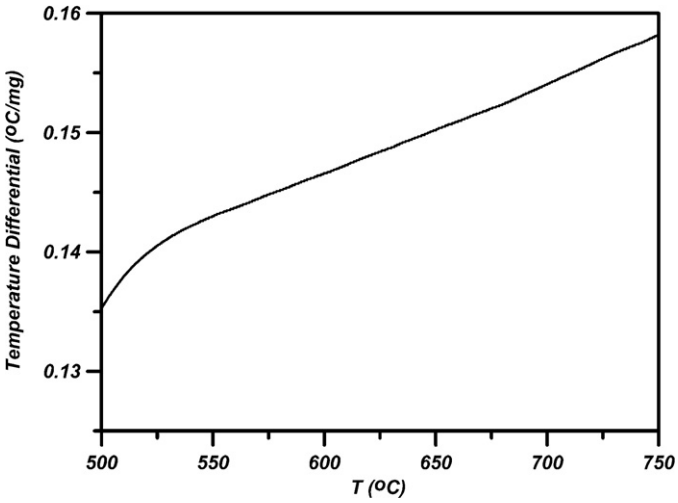

Fig. 8. DTA curve for the 10E5NSB been annealed at 650 °C for 300 h.

doping concentration is also observed in ENSB system. At fixed dopant ratio, the conductivity decreases with increasing of doping concentration, which agrees with previous report. Activation energy of migration of the oxygen through the vacancy-exchange mechanism is calculated by the following empirical equation:

$$\sigma T = A \exp\left(\frac{E_a}{kT}\right), \quad (3)$$

where σ is oxygen ion conductivity, T is absolute temperature, A is a pre-exponential term, k is Boltzmann constant and E_a is activation energy of the oxygen migration. The measured energies and their deviations are listed in Table 1. The reported results of the ESB are added for comparisons.

The conductivities in Fig. 4 experience a slope change around 600 °C. Literature has reported that doped δ-Bi_2O_3 goes through an oxygen-vacancies order-disorder transition, which is reflected by a change of activation energy, at about 600 °C.[4,11,23] When the temperature is greater than the order-disorder temperature, the disorder state of oxygen vacancies is maintained, so the migration of oxygen through the O–V_O exchange in fluorite structure is controlled by how difficult to overcome the edge blocking effect.[11,26,27] When the temperature is below the order-disorder temperature, oxygen-vacancies tend to form short-range ordering in the compositions with M-O (M is Er^{3+} or Nb^{5+} smaller ions). The edge blocking does not play the major role in the cases, instead, the bond strength of M-O controls the migration of oxygen.[11]

For three ENSB compositions (6.7E3.3NSB, 10E5NSB, 11.25E3.75NSB), the activation energy of high-temperature region is increased with the doping concentration. However, the 6.7E3.3NSB and 10E5NSB have very close value of the activation energy. It is due to that the lattice constant of 6.7E3.3NSB (5.523 Å) and 10E5NSB (5.519 Å) are very close, the edge blocking effect of both is almost the same. The activation energy of low-temperature region shows similar trend, which agrees with the previous report.[11,15]

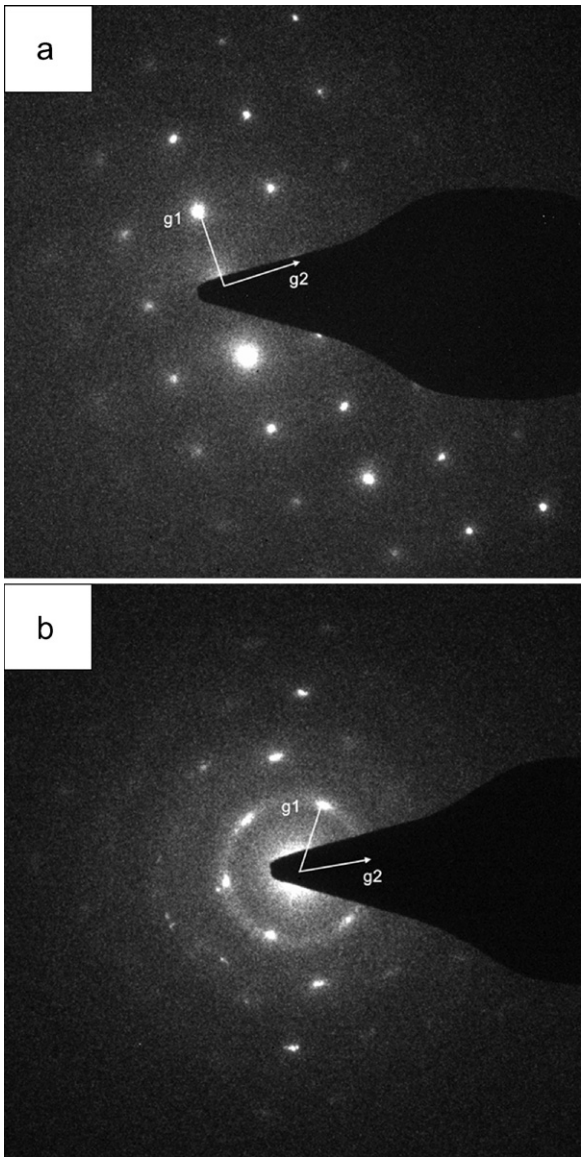

Fig. 9. Diffraction patterns obtained for the 10E5NSB after 300 h annealing at 650 °C. (a) ⟨0 0 1⟩ zone: g1 and g2 correspond to the {2 0 0} family of cubic δ-Bi_2O_3 (JCPDS card 52-1007). (b) ⟨1 1 0⟩ zone: g1 and g2 correspond to the {1 1 1} and {2 0 0} family of cubic δ-Bi_2O_3. Long range orderings along ⟨1 0 0⟩, ⟨1 1 0⟩, or ⟨1 1 1⟩ directions are not observed.

3.3. Long-term stability

Three samples, 6.7E3.3NSB, 10E5NSB and 11.25E3.75NSB, have been tested at 650 °C for 20–300 h. The evolution of phases identified by XRD is shown in Fig. 5. In Fig. 5(a), the single δ-phase shows wider diffraction peaks, implying additional fluorite structure with slightly different lattices constant appeared from 20 h annealing. After 100 h annealing, the α-phase appeared and co-existed with δ-phase. In Fig. 5(b), the 10E5NSB sample has no obvious second phase formation after 100 h annealing test. Nevertheless, only trace of γ-phase appears after 300 h. Similar phase transformation in Fig. 5(c) for the composition 13.3E6.7NSB, additional γ-phase

Table 1
Activation energies of various Er and Nb co-doped Bi_2O_3 sample in the specified temperature region.

Compositions	Activation energies (eV)		Reference
	High temperature (≥600 °C)	Low temperature (≤600 °C)	
6.7E3.3NSB	0.89 ± 0.03	1.17 ± 0.09	This study
10E5NSB	0.89 ± 0.03	1.19 ± 0.02	
13.3E6.7NSB	1.07 ± 0.03	1.18 ± 0.03	
15ESB	0.58 ± 0.02	1.08 ± 0.03	Verkerk et al., 1980
20ESB	0.64 ± 0.03	1.190 ± 0.005	

Note: the deviation of energy value is estimated in 95% confident interval.

in the 13.3E6.6NSB after 100 h aging was detected, and the content increased continuously with time.

Fig. 6(a) shows the SEM image of the polished surface of as-sintered ENSB sample and Fig. 6(b)–(d) show the as-annealed surface images of the samples by 650 °C for 300 h. The as-sintered sample presents dense surface and only trace of tiny pores are observed. Plenty of platy features in Fig. 6(b) are noted in Bi_2O_3-based grains to be α-phase. But some grains are free from the platy feature. The SEM images of annealed 10E5NSB in Fig. 6(c) shows a few newly grown features, two pointed grains at grain boundary are found. Those can be the γ-grains precipitated from matrix. The SEM image of annealed 13.3E6.7NSB in Fig. 6(d) presents submicron γ-grains in matrix. According to the results of XRD and SEM, 10E5NSB is relatively stable than the other two while annealing at 650 °C.

The long-term conductivity test annealing at 650 °C of the stable sample 10E5NSB is shown in Fig. 7. The annealing result presents a fast degradation of conductivity in early time. The conductivity has degraded continuously to 1.6×10^{-2} S cm^{-1} with time until ∼150 h. In order to clarify the mechanism of conductivity degradation, DTA and TEM have been carried on for analysis. According to the report by Jiang et al.[14] a vacancy ordering-disordering transformation involved the entropy variation and an endothermic peak appeared in their DTA result during heating for vacancy-ordered samples.

Fig. 8 shows the DTA result of 10E5NSB sample which has been annealed at 650 °C for 300 h. No any endothermic peak around 600 °C is observed in the 10E5NSB sample. Additional TEM diffraction patterns were obtained in search of the evidence of vacancy ordering. Fig. 9(a) was the pattern on ⟨0 0 1⟩ zone, where g1 and g2 correspond to the {2 0 0} family of cubic δ-Bi_2O_3. Fig. 9(b) was on ⟨1 1 0⟩ zone, where g1 and g2 correspond to the {1 1 1} and {2 0 0} family of cubic δ-Bi_2O_3, respectively. Both diffractions revealed no faint superlattice reflections. Although long-range vacancy ordering and order-disorder endotherm were absent in 10E5NSB, the immediate conductivity decay within the first 50 h at 650 °C clearly indicated dominated by the formation of secondary phase, i.e. γ-structure.

Other possibility, short range ordering by structural relaxation, was proposed in the study of long term annealing of Bi_2O_3–Er_2O_3–PbO by Webster et al.[28] Their DTA curve and TEM diffraction of 27E(Er)3PbSB did not reveal endothermic peaks nor superlattice reflections in ⟨1 1 1⟩ direction until after 1000 h annealing. They suggested conductivity decade was due to short-range ⟨1 1 1⟩ oxide-ion sublattice ordering.[28]

Since "true" stability of most dopant-stabilized δ-Bi_2O_3 is questioned by Watanabe,[22] His recent work reported that[24] the compositional domain at 24.5E(Er)5WSB showed first fully stabilized δ-Bi_2O_3, which exhibited a merely 1% conductivity decay up to a period of 800 h annealing at 600 °C. It is believed that the temperature-time dependences of the conductivity behaviors demonstrated relaxation phenomenon could be a matter of kinetics, similar to the suggestion by Jung et al.[29]

4. Conclusion

Bi_2O_3-based materials are stabilized to δ-phase with total doping concentration of (Er + Nb) reduced from 20 mol.% to 10 mol.% with double dopants in a ratio of Er/Nb = 2. The relative content of Er and Nb induced two-step lattice contraction behavior when TDC is less than 15 mol.%.

For the composition 6.7E3.3NSB with the best electric conductivity in short term aspect, the conductivities were 0.351, 0.106, 1.26×10^{-2} S cm^{-1} at 700 °C, 600 °C and 500 °C. But this sample grew appreciable amount of α-phase and the conductivity decreased dramatically after annealing at 650 °C for 300 h. In comparison, only trace of γ-phase was observed in 10E5NSB sample. The sample degraded to 1.6×10^{-2} S cm^{-1} at 650 °C in 150 h and kept nearly the same level of electric conductivity until 300 h. No long-range vacancy ordering by DTA and TEM was observed in this sample which had been annealed at 650 °C for 300 h. The slow phase transformation of δ-to-γ structure may be responsible for the conductivity degradation.

Acknowledgements

The authors like to thank the funding from National Science Council (NSC99-2221-E-002-113-MY2) in Taiwan, and helpful discussion with professors Wachsman and Abrahams during their visit to Taiwan.

References

1. Sammes NM, Tompsett GA, Nafe H, Aldinger F. Bismuth based oxide electrolytes—structure and ionic conductivity. *J Eur Ceram Soc* 1999;**19**:1801–26.
2. Kharton VV, Naumovich EN, Yaremchenko AA, Marques FMB. Research on the electrochemistry of oxygen ion conductors in the former Soviet Union. *J Solid State Electrochem* 2001;**5**:160–87.

3. Kharton VV, Marques FMB, Akinson A. Transport properties of electrolyte ceramics: a brief review. *Solid State Ionic* 2004;**174**:135–49.
4. Boyapati S, Wachsman ED, Jiang N. Effect of oxygen sublattice ordering on interstitial transport mechanism and conductivity activation energies in phase-stabilized cubic bismuth oxides. *Solid State Ionic* 2001;**140**:149–60.
5. Conflant P, Follet-Houttemane C, Drache M. The Bi_2O_3–Sm_2O_3 system: phase diagram and electrical properties. *J Mater Chem* 1991: 649–53.
6. Drache M, Roussel P, Wignacourt JP. Structures and oxide mobility in Bi–Ln–O materials: heritage of Bi_2O_3. *Chem Rev* 2007;**107**:80–96.
7. Esaka T, Iwahara H. Oxide ion and electron mixed conductor in the fluorite-type cubic solid solution in the system Bi_2O_3–$Tb_2O_{3.5}$. *J Appl Electrochem* 1985;**15**:447–51.
8. Iwahara H, Esaka T, Sato T, Takahashi T. Formation of high oxide ion conductive phases in the sintered oxides of the system Bi_2O_3–Ln_2O_3 (Ln = La–Yb). *J Solid State Chem* 1981;**39**:173–80.
9. Takahashi T, Iwahara H, Arao T. High oxide ion conduction in sintered oxides of system of system Bi_2O_3–Y_2O_3. *J Appl Electrochem* 1975;**5**:187–95.
10. Takahashi T, Esaka T, Iwahara H. High oxide ion conduction in sintered oxides of system of system Bi_2O_3–Gd_2O_3. *J Appl Electrochem* 1975;**5**:197–202.
11. Verkerk MJ, Burggraaf AJ. High oxygen ion conduction in sintered oxides of the Bi_2O_3–Ln_2O_3 system. *Solid State Ionics* 1981;**3–4**:463–7.
12. Takahashi T, Iwahara H, Esaka T. High oxide ion conduction in sintered oxide of the system Bi_2O_3–M_2O_5. *J Electrochem Soc* 1977;**124**:1563–9.
13. Meng GY, Chen CS, Han X, Yang PH, Peng DK. Conductivity of Bi_2O_3-based oxide ion conductor with double stabilizers. *Solid State Ionics* 1988;**28**:533–8.
14. Jiang N, Wachsman ED, Jung S. A higher conductivity Bi_2O_3-based electrolyte. *Solid State Ionics* 2002;**150**(6):347–53.
15. Jung DW, Duncan KL, Wachsman ED. Effect of total dopant concentration and dopant ratio on conductivity of $(DyO_{1.5})_x$–$(WO_3)_y$–$(BiO_{1.5})_{1-x-y}$. *Acta Mater* 2010;**58**:355–63.
16. Kruidhof H, de Vries KJ, Burggraaf AJ. Thermochemical stability and nonstoichiometry of yttria-stabilized bismuth oxide solid solutions. *Solid State Ionics* 1990;**37**:2135.
17. Verkerk MJ, Burggraaf AJ. High oxygen ion conduction in sintered oxides of the Bi_2O_3–Dy_2O_3 system. *J Electrochem Soc* 1981;**128**: 75–82.
18. Watanabe A. Phase relations of hexagonal and cubic phases in Holmia-doped bismuth sesquioxide, $Bi_{2-2x}Ho_{2x}O_3$ (x = 0.205–0.245). *Solid State Ionics* 1989;**34**:35–9.
19. Fung KZ, Chen J, Virka AV. Effect of aliovalent dopants on the kinetics of phase-transformation and ordering in Re_2O_3–Bi_2O_3 (Re = Yb, Er, Y, or Dy) solid-solutions. *J Am Ceram Soc* 1993;**76**:2403–18.
20. Fung KZ, Baek HD, Virka AV. Thermodynamic and kinetic considerations for Bi_2O_3-based electrolytes. *Solid State Ionics* 1992;**52**:199–211.
21. Fung KZ, Virka AV. Phase-stability, phase-transformation kinetics, and conductivity of Y_2O_3–Bi_2O_3 solid electrolytes containing aliovalent dopants. *J Am Ceram Soc* 1991;**74**:1970–80.
22. Watanabe A. Is it possible to stabilize δ-Bi_2O_3 by an oxide additive? *Solid State Ionics* 1990;**40**(1):889–92.
23. Jiang N, Wachsman ED. Structural stability and conductivity of phase-stabilized cubic bismuth oxides. *J Am Ceram Soc* 1999;**82**(11): 3057–64.
24. Watanabe A, Sekita M. Stabilized δ-Bi_2O_3 phase in the system Bi_2O_3–Er_2O_3–WO_3 and its oxide-ion conduction. *Solid State Ionics* 2005;**176**:2429–33.
25. Weng CH, Wei WCJ. Synthesis and properties of homogeneous Nb-doped bismuth oxide. *J Am Ceram Soc* 2010;**93**(10):3124–9.
26. Huang, C. W., Wei, W. C. J., and Chen, C. S. Atomic simulation of oxygen in fluorite structure. *J Eur Ceram Soc*, doi:10.1016/j.jeurceramsoc.2011.05.029.
27. Huang CW, Wei WCJ, Chen CS. Simulation of atomic-scale defects in the clustering and oxygen jumping process of 8 mol% yttria-stabilized zirconia. *J Ceram Proc Res* 2010;**11**(6):641–7.
28. Webster NAS, Ling CD, Raston CL, Lincoln FJ. The structural and conductivity evolution of fluorite-type Bi_2O_3–Er_2O_3–PbO solid electrolytes during long-term annealing. *Solid State Ionics* 2008;**79**:697–705.
29. Jung DW, Duncan KL, Camaratta MA, Lee KT, Nino JC, Wachsman ED. Effect of annealing temperature and dopant concentration on the conductivity behavior in $(DyO_{1.5})_x$–$(WO_3)_y$–$(BiO_{1.5})_{1-x-y}$. *J Am Ceram Soc* 2010;**93**:1384–91.